Conceptual design of the Radial Gamma Ray Spectrometers system for α particle and runaway electron measurements at ITER

M. Nocente[1,2], M. Tardocchi[2], R. Barnsley[3], L. Bertalot[3], B. Brichard[4], G. Croci[1,2], G. Brolatti[5], L. Di Pace[5], A. Fernandes[6], L. Giacomelli[2], I. Lengar[7], M. Moszynski[8], V. Krasilnikov[3], A. Muraro[1,2], R. C. Pereira[6], E. Perelli Cippo[2], D. Rigamonti[1,2], M. Rebai[1,2], J. Rzadkiewicz[8], M. Salewski[9], P. Santosh[3], J. Sousa[6], I. Zychor[8] and G. Gorini[1,2]

[1]Dipartimento di Fisica "G. Occhialini", Università di Milano-Bicocca, Milano, Italy
[2]Istituto di Fisica del Plasma, Consiglio Nazionale delle Ricerche, Milano, Italy
[3]ITER organization, St Paul Lez Durance Cedex, France
[4]Fusion for Energy, Barcellona, Spain
[5]ENEA C. R. Frascati, Dipartimento FSN, Frascati, Italy
[6]Instituto de Plasmas e Fusão Nuclear, Instituto Superior Técnico, Universidade de Lisboa, 1049-001 Lisboa, Portugal
[7]Jozef Stefan Institute, Ljubljana, Slovenia
[8]National Center for Nuclear Research, NCBJ, Swierk, Warsaw, Poland
[9]Technical University of Denmark, Department of Physics, Kgs. Lyngby, Denmark

Corresponding Author: massimo.nocente@mib.infn.it

Abstract:

We here present the principles and main physics capabilities behind the design of the Radial Gamma Ray Spectrometers (RGRS) system for alpha particle and runaway electron measurements at ITER. The diagnostic benefits from recent advances in gamma-ray spectrometry for tokamak plasmas and combines space and high energy resolution in a single device. The RGRS system as designed can provide information on α particles on a time scale of 1/10 of the slowing down time for the ITER 500 MW full power DT scenario. Spectral observations of the 3.21 and 4.44 MeV peaks from the $^9\mathrm{Be}(\alpha, \mathrm{n}\gamma)^{12}\mathrm{C}$ reaction make the measurements sensitive to α particles at characteristic resonant energies and to possible anisotropies of their slowing down distribution function. An independent assessment of the neutron rate by gamma-ray emission is also feasible.
In case of runaway electrons born in disruptions with a typical duration of 100 ms, a time resolution of at least 10 ms for runaway electron studies can be achieved depending on the scenario and down to a current of 40 kA by use of external gas injection. We find that the bremsstrahlung spectrum in the MeV range from confined runaways is sensitive to the electron velocity space up to $E \approx$ 30-40 MeV, which allows for measurements of the energy distribution of the runaway electrons at ITER.

1 Introduction

The ITER project aims at demonstrating fusion power production with a gain of ten and for a duration of about 400 s when the current is driven by the Ohmic transformer. On the path towards this highly ambitious goal, ITER will explore, for the first time, the physics of a burning plasma, i.e. a regime where the heating fraction due to the alpha particles exceeds that of the external auxiliary heating systems. Besides, it will also show that plasma operations at unprecedented high performance can be conducted in a reliable and safe way, for example by avoiding damage of the machine first wall due to the generation of an uncontrolled beam of runaway electrons. The design of a system that can simultaneously be used to measure α particles and runaway electrons is thus instrumental to the very core of the ITER mission. The observation of spontaneous gamma-ray emission from reactions between confined fast ions, such as α particles, and impurities is the natural way to probe the energy distribution and spatial profile of the energetic ions [1, 2, 3, 4]. On the other hand, bremsstrahlung emission induced by confined or de-confined runaway electrons can be used to understand their energy distribution and birth/losses in the different phases of the plasma discharge [5, 6]. As both emissions occur in the MeV range, a single, well calibrated system of gamma-ray spectrometers can be in principle used to fulfil both highly important tasks. According to the ITER needs [7, 8], the desired role of gamma-ray spectrometry measurements is to act as primary diagnostics for runaway electrons and α particle studies and to provide backup or supplementary information on a number of parameters related to fast ions, neutron emission and the fuel ion ratio, as specified in Table I.

In this paper we present the conceptual design of the Radial Gamma-Ray Spectrometer (RGRS) system for ITER. The system consists of a set of gamma-ray spectrometers and carefully collimated, radial lines of sight designed for installation in a few of the channels of the Radial Neutron Camera (RNC) system for neutron emission profile measurements at ITER [9].

Here we present the principles and modelling results that have shaped the system, we evaluate the parameter range where our device can provide useful information both on runaway electrons and α particles and we discuss the observational possibilities offered by RGRS for physics studies. Our design is based on the present experience with gamma-ray measurements at the JET tokamak, but it also benefits from the larger space available for RGRS at ITER compared to the JET radial gamma-ray camera. The system has been designed to meet the main primary diagnostic requirements of gamma-ray spectroscopy (see table I) and this is the focus of the present paper and the driver of our conceptual design. Although RGRS may also contribute to meeting the backup and supplementary requirements of gamma-ray spectrometry, they are not the focus of this work and will be the subject of future studies.

The paper is organised as follows. A summary on the state of the art of gamma-ray measurements and their use in present day tokamaks is provided in sections 2 and 3. Section 4 presents our modelling assumptions and calculated gamma-ray emission from α particles, where the aim is here to determine associated challenges and to find solutions that allow for measurements on a time scale of relevance for α particle slowing down

TABLE I: Primary, backup and supplementary diagnostic roles for gamma-ray spectrometry at ITER as identified in [7, 8]. The time resolution and accuracy requirements are specified for the primary diagnostic roles only.

Role	Measurement parameter
Primary	Maximum energy of runaway electrons (range: 1-100 MeV; time resolution: 10 ms; accuracy: 20%)
Primary	Runaway electron current after thermal quench (range: 1-15 MA; time resolution: 10 ms; accuracy: 30%)
Primary	Runaway electron current for failed breakdown (range: 1-5 MA; time resolution: 10 ms; accuracy: 50 kA)
Primary	Alpha Density Profile (range: $10^{17} - 2 \cdot 10^{18}$ m^{-3}; time resolution: 100 ms; spatial resolution: a/10; accuracy: 20%)
Backup	Neutron and alpha source profile
Backup	Profile of ^{3}He concentration
Supplementary	n_T/n_D in the plasma core
Supplementary	Be, C, O relative concentrations
Supplementary	Alpha particle energy spectrum
Supplementary	p, D, T, ^{3}He energy spectrum
Supplementary	Fractional content $Z \leq 10$

studies. The RGRS detector specifications defined by these requirements are then used to determine the capability of the system to also measure runaway electrons in disruptions at currents from 40 kA to 10 MA in section 5. To this end, we also discuss the models that have been adopted to evaluate bremsstrahlung emission from runaway electrons described by an arbitrary distribution function. This is done by extending the GENESIS [10, 11] Monte Carlo code, initially developed to evaluate gamma-ray emission from nuclear reactions, to bremsstrahlung in the gamma-ray energy range from confined MeV electrons. The velocity space sensitivity of gamma-ray emission measured with RGRS at ITER is discussed by means of weight functions both for α particles and runaway electrons.

2 Role of γ ray measurements at ITER

Gamma-ray measurements at ITER have primarily two aims. The first is to measure the profile and energy distribution of α particles born from deuterium-tritium (DT) reactions. This is obtained by observations of the 4.44 MeV gamma-ray emission from the $^9\mathrm{Be}(\alpha, \mathrm{n}\gamma)^{12}\mathrm{C}$ reaction that naturally occurs in the plasma between fusion born α particles

and ^{9}Be impurities [12]. The latter come from the erosion of the machine first wall and are found in the plasma at typical concentrations around 1%. 4.44 MeV gamma-ray emission can in principle provide information on the α particle profile and energy distribution [2] and is therefore of key importance. The detection of 4.44 MeV gamma-rays is obtained by observation of the intensity and shape of the full energy peak in the pulse height spectrum resulting from the interaction of the radiation with the spectrometer [12, 10], i.e. by performing measurements at high resolution (say, 1.5% or better) in a relatively narrow energy band of the gamma-ray spectrum.
The second goal of gamma-ray measurements at ITER is the detection and study of runaway electrons (REs) that may be generated, for example, during disruptions. Gamma-rays are in this case born from bremsstrahlung emission, that occurs either when a beam of confined runaway electrons interacts with the bulk plasma (thin target bremsstrahlung) or if runaways that get lost from the plasma hit a metal structure at the tokamak edge (thick target bremsstrahlung). In both cases, besides the intensity, there is interest in measuring the MeV range spectrum of such bremsstrahlung emission as this carries information on the energy distribution and current of the REs [5]. In this paper, we focus only on thin target bremsstrahlung emission. Unlike gamma-rays from the $^9\mathrm{Be}(\alpha, \mathrm{n}\gamma)^{12}\mathrm{C}$ reaction with a well defined energy (4.44 MeV), the bremsstrahlung process generates radiation with a continuous energy spectrum (see section 5) and that mostly interacts with the detector via Compton scattering. Experimentally, it is therefore the broadband shape of the spectrum - and not only a narrow energy band - that is of relevance for RE studies with gamma-ray spectrometers.

3 State of the art and main RGRS features

The design of the RGRS system at ITER is based on the experience built at the Joint European Torus (JET), where the most advanced set of gamma-ray spectrometers to date is installed. At JET, two separate systems have been developed to obtain spatial and energy information on the energetic particles responsible for gamma-ray emission:

a) a set of large high resolution spectrometers [13], which are installed along one vertical and one horizontal lines of sight. The most advanced spectrometers used at JET are $LaBr_3$ (scintillator size: 3 inches x 6 inches, diameter x height)[14] and high purity Germanium (HpGe)[10, 12].

b) a gamma-ray camera [2], i.e. a set of detectors at the end of collimated lines of sight which are used to determine the map of the gamma-ray emission in the poloidal plane by tomographic inversion. Of special importance in view of ITER is the recent upgrade of the detectors discussed in [15, 16, 17] and that will allow to provide, for the first time, gamma-ray tomographic measurements in plasmas with tritium in the forthcoming campaigns.

As gamma-ray diagnostics were not integrated in the initial JET design, large detectors at sufficiently high energy resolution to allow for measurements of the peak shape broadening along each channel of the gamma-ray camera cannot be developed, due to space

limitation. For this reason, at JET, profile and energy distribution measurements are accomplished by two *separate* systems, the camera and the high resolution detectors, respectively.
Contrary to JET, ITER has a larger volume and the RGRS system is designed in a integrated way with the RNC. Therefore, a system that combines space and energy distribution measurements of the energetic particles can be devised by displacing high resolution detectors in a camera assembly. This is the main principle behind the RGRS design.
The location of the system, as well as the number of lines of sight available, were determined by interfacing constraints with the RNC. These have resulted in the location of the system shown in figure 1, where RGRS is found between the biological shielding and the high resolution neutron spectrometer (HRNS). RGRS has up to 8 radial sightlines shared with the RNC. In terms of spatial coverage in the poloidal plane, this is limited to a radial region $r < a/3$, where $a = 2$ m is the machine minor radius. The radial limitation comes from the unavailability of the RNC in-port lines of sight for RGRS. Clearly, some coverage of the region $r > a/3$ would be desirable, but this requires the installation of gamma-ray detectors in the in-port region of figure 1 and it is presently not allowed by the RNC design. Besides, in-port detectors are exposed to a significantly higher background radiation load and, provided gamma-ray measurements are still possible in that location, a completely different detector concept would have to be envisaged, which is outside the scope of the present project.

4 Alpha particle studies with RGRS

4.1 Modelling

In order to determine the capability of RGRS to study α particles in ITER DT plasmas, we have calculated the expected signal at 4.44 MeV from the $^9\mathrm{Be}(\alpha, \mathrm{n}\gamma)^{12}\mathrm{C}$ reaction for the full power 500 MW ITER scenario using a semi-analytical approach. Plasma parameters are shown in figure 2 and were taken from [18], with an assumed ^{9}Be concentration of 1%. The steady state alpha particle distribution function was evaluated from the position dependent alpha particle source ($\alpha\mathrm{s\ m^{-3}s^{-1}}$) of [18] based on a 1-dimensional Fokker-Planck model (see eq. (4) of [19]) and using local plasma parameters to evaluate the Spitzer slowing down time at each plasma position. This was the input for the GENESIS code [11, 10] to evaluate the local gamma-ray emissivity $y_\gamma(r, z)$ $[\gamma \cdot \mathrm{s}^{-1} \cdot \mathrm{m}^{-3}]$ in the poloidal cross section. The result is displayed by the map of figure 3, where 4.44 MeV gamma-ray emission is compared to that from fusion born 14 MeV neutrons. The comparison shows that the plasma produces about 40000 neutrons per 4.44 MeV gamma-ray, which requires to use suitable attenuators, see the next paragraph.

From the local neutron or gamma-ray emissivity $y_{n,\gamma}(r, z)$, and assuming narrow sightlines, the flux $\phi[\gamma \cdot \mathrm{s}^{-1} \cdot \mathrm{cm}^{-2}]$ impinging on each detector of the RGRS system was estimated by the formulas of [20], i.e.

$$\phi_{n,\gamma} = \frac{1}{16} \left(\frac{d_C}{L} \right)^2 \int_\lambda y_{n,\gamma}(s) ds \tag{1}$$

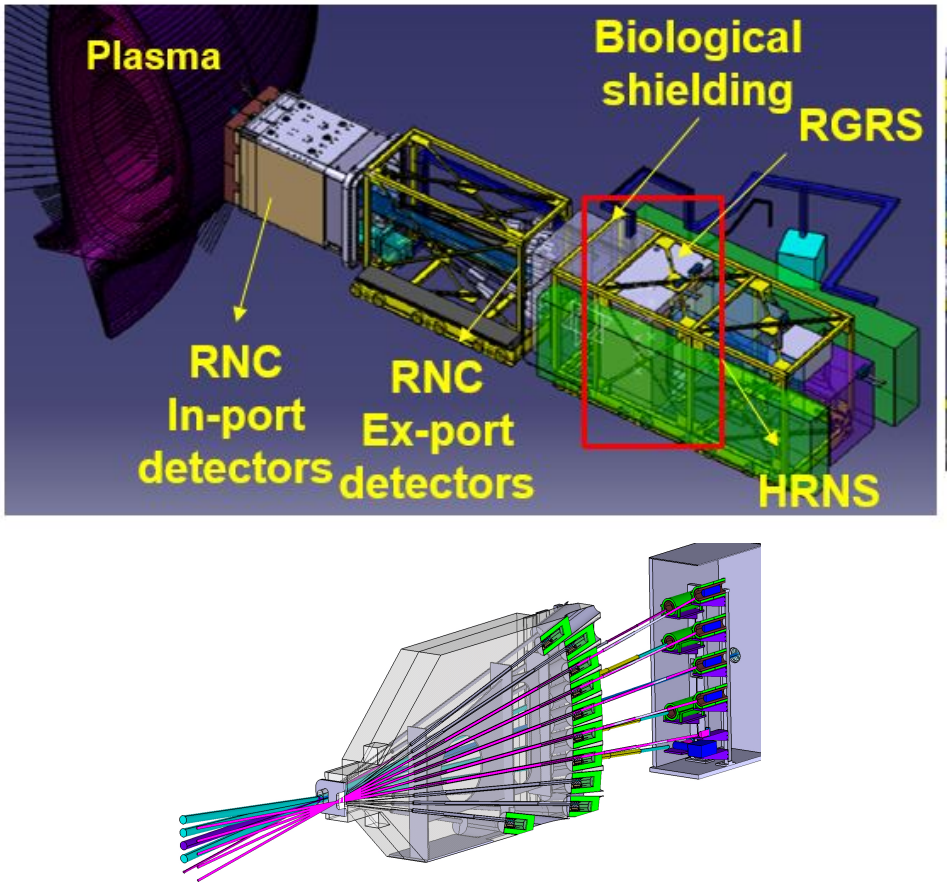

FIG. 1: (top) Schematics of the RGRS position with respect to the Radial Neutron Camera (RNC), the High Resolution Neutron Spectrometer (HRNS) and ITER plasmas. (bottom) Cross section of the diagnostic port of RGRS with its lines of sight. The RGRS detectors are shown at the end of each line of sight (blue and green) and sit behind the RNC ex-port detectors (grey and green)

where λ is the line of sight, d_C is the collimator diameter and L its length. The counting rate r at the detector is finally given by

$$r_{n,\gamma} = \phi \cdot \pi/4 \cdot d_C^2 \epsilon \tag{2}$$

where ϵ is here either the detector full peak efficiency at 4.44 MeV, or the 14 MeV neutron detector efficiency of $LaBr_3$ [21]. The subscripts n and γ in equation 2 indicate neutrons and gammas, respectively. By combining equations 1 and 2 it is seen that r scales as d_C^4. Detailed MCNP simulations show that equations 2 and 1 provide an accuracy between 20% and 30% with respect to a detailed transport model. This is well within the uncertainty on simulated plasma parameters for the ITER DT scenario and justifies our simplified, semi-analytical approach.

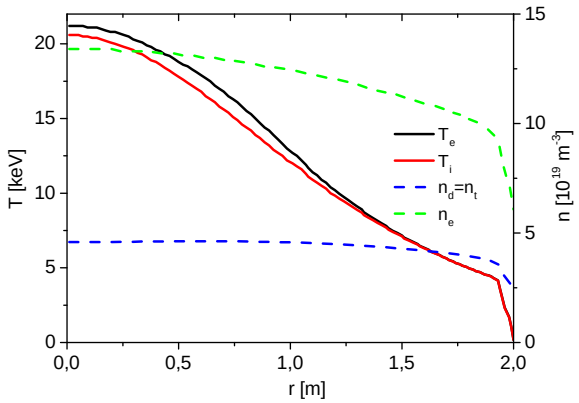

FIG. 2: Plasma parameters of the 500 MW DT ITER scenario used as input for our calculations and as a function of the minor radius r in the poloidal cross section. Ion (T_i) and electron (T_e) temperatures are shown to the left. The electron density (n_e), as well as the densities of deuterium (n_d) and tritium (n_t), are shown to the right

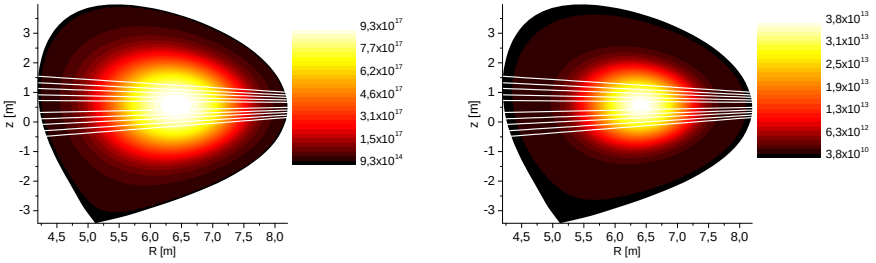

FIG. 3: Calculated 14 MeV neutron (left) and 4.44 MeV γ-ray (right) emissivities (particles/m^3/s) in the poloidal plane for the ITER 500 MW DT scenario. White lines indicate the RGRS observation chords.

4.2 Detector solutions and interfacing issues

From equations 1 and 2 the expected counting rate depends on L, d_C and ϵ, which are set by the collimator (L and d_C) and the detector choice (ϵ). The upper limit on ϵ is determined by the largest, high resolution scintillator crystal presently available, which is the 3"x6" $LaBr_3$ installed at JET and this is also adopted for RGRS. For this detector, we obtain $\epsilon \approx 20\%$. The RNC design sets L= 3 m, while d_C can be (at most) of a few cm. If we use d_C=4 cm and assume to exploit all of the flux impinging at the RNC position, we obtain r_γ ≈120 kHz in the central channel of RGRS if no attenuation occurs along the line of sight. However, we also correspondingly find $r_n \approx 2.4 \cdot 10^{10}$ Hz given that $\epsilon \approx 1$ for the detection of 14 MeV neutrons by $LaBr_3$ [21]. This shows that the main challenge for 4.44 MeV gamma-ray measurements in ITER DT plasmas is the need to overcome the background induced by 14 MeV neutrons, either because they directly interact with

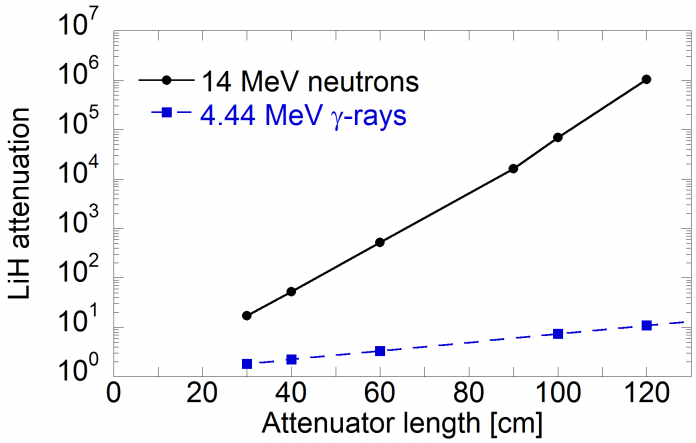

FIG. 4: LiH attenuation factor for 14 MeV neutrons (circles) and 4.44 MeV gamma-rays (squares) as a function of the attenuator length.

the scintillator, or since they induce gamma-ray background in their thermalization path by multiple collision with the tokamak structures. Clearly, a background counting rate of $\approx 10^{10}$ Hz would paralyse the detector and make any measurement impossible.
In order to reduce the background from direct 14 MeV neutron interactions with the crystal, the RGRS design includes the use of LiH[22] as attenuator in front of each detector. MCNP simulations show (figure 4), and experiments at nuclear accelerators confirm[22], that LiH samples of some tens of centimeter can attenuate 14 MeV neutrons by orders of magnitude, while reducing the 4.44 MeV gamma-ray flux by up to a factor 10. For this reason, the RGRS design includes a 120 cm sample of LiH in front of each of the detectors. The sample is placed in the line of sight cavity inside the biological shielding. When LiH is included in the RGRS model, we find $r_\gamma \approx 12$ kHz (and an overall detector load from 4.44 MeV gamma-rays of 60 kHz). For comparison, $r_n \approx 10$ kHz. This background is, however, spectrally distributed mostly at $E_\gamma < 3$ MeV and only about 40 Hz falls in the region of the 4.44 MeV peak. The background induced by direct 14 MeV neutron interactions with the crystal is therefore negligible after the attenuators.

The main source of background is the gamma-ray load induced by 14 MeV neutrons that thermalize by multiple collisions with the tokamak structures, where an important contribution comes from capture of thermal neutrons by the shielding materials of the RNC. In order to partially overcome this gamma-ray background, we have designed a shielding based on a combination of concrete and iron that are meant to attenuate the radiation load coming from the sides of the detector. Figure 5 shows a calculation of the overall pulse height spectrum measured by the 3"x6" $LaBr_3$ detector in the region $E_\gamma > 3$ MeV, which is of interest for physics studies [1, 4] (a description of the prominent features of the spectrum is given in the next section). We find that the peak to background ratio at 4.44 MeV is ≈ 2 and the overall counting rate is 3.5 MHz, which is well within the capability of $LaBr_3$ [14]. If, instead, HpGe were to be used, we would measure a counting rate of about 1.5 MHz due to its reduced size (3"x3", diameter x height) and,

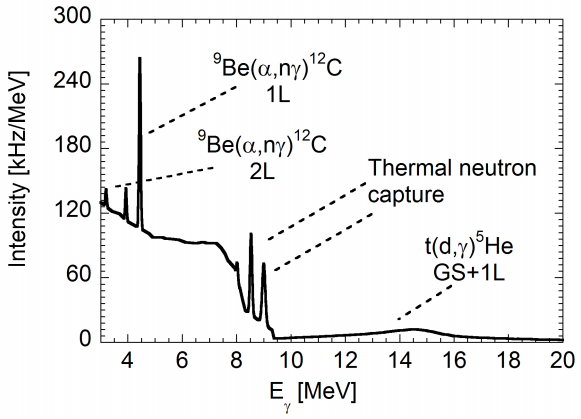

FIG. 5: Calculation results on the pulse height spectrum expected on $LaBr_3$ *for the 500 MW DT scenario at ITER. Peaks at 4.44 and 3.21 MeV come from the de-excitation of the first (1L) and second (2L) excited states of* ^{12}C *produced in the* $^9\mathrm{Be}(\alpha, \mathrm{n}\gamma)^{12}\mathrm{C}$ *reaction, respectively. The most prominent features of the background are the two peaks at 8.5 and 9 MeV and that come from nuclear capture of thermal neutrons. The broad structure at* $E_\gamma > 10$ *MeV comes from the* $\mathrm{t}(\mathrm{d}, \gamma)^5\mathrm{He}$ *reaction that leaves* ^5He *in its ground (GS) or first (1L) excited state.*

hence, efficiency. This is, however, at the limit of the capabilities of HpGe, for which measurements at counting rates up to about 1 MHz and 40% throughput have so far been demonstrated [23]. Still, HpGe can be handy for measurements at enhanced energy resolution in lower power scenarios or provided that some further gamma-ray attenuator (eg. few centimeters of lead) is added in the 500 MW DT scenario so to reduce the counting rate by a factor 2.

4.3 Physics studies

Among the primary aims of RGRS is to provide information on the α particle profile, which is attained by measurements of the intensity of the 4.44 MeV peak along each of the channels of the system. The accuracy of the measurements depends on Poisson statistics and is improved by a larger number of counts. This is obtained by a longer integration time, which sets the time resolution Δt at which physics information can be retrieved.

The total number of counts T falling in the region of the 4.44 MeV peak is made of contributions from the signal S and the gamma-ray background B, i.e $T = S + B$, and both are subject to Poisson statistics. B is in turn a fraction f of the signal, where f is the inverse of the signal-to-background ratio. Hence $S = T/(1+f)$ and $B = f/(1+f) \cdot T$. If we prescribe an accuracy ϵ on the signal, then

$$\frac{\sigma_S}{S} < \epsilon \tag{3}$$

where $\sigma_S = \sqrt{\sigma_T^2 + \sigma_B^2} = \sqrt{T + B}$, so that the total number of counts that we need in order to reach the accuracy ϵ is

$$T \geq 1/\epsilon^2(1+f)(1+2f) \tag{4}$$

The time resolution is then

$$\Delta t = T/r \tag{5}$$

where r is the total (signal plus background) counting rate in the region of the 4.44 MeV peak.

Since $f = 0.5$, if we set ϵ=20% and $LaBr_3$ as detector, we obtain Δt=17 ms for the central channel. This compares with a typical α particle slowing down time τ_α of about 1 s and implies a time resolution better than $\tau_\alpha/10$. Concerning the edge channels of RGRS, our calculations show that they receive a reduced counting rate by 30% with respect to the central channel, so that α particle profile information in the whole $r < a/3$ region and 10% accuracy is attainable with a time resolution better than $\tau_\alpha/10$. Here we also note that a time resolution of $\tau_\alpha/10$ is possible up to an accuracy level of 5%.

The 4.44 MeV peak from the $^9\mathrm{Be}(\alpha, \mathrm{n}\gamma)^{12}\mathrm{C}$ reaction is the main source of information on α particles through gamma-ray spectrometry and results from the decay of the first excited state of ^{12}C. There are, however, two further emissions that can be exploited to gain information on α particles. The first is a peak at 3.21 MeV that is manifested when ^{12}C from the $^9\mathrm{Be}(\alpha, \mathrm{n}\gamma)^{12}\mathrm{C}$ reaction is born in its second excited state at 7.65 MeV and decays by a transition from the second to first level. The intensity of this emission is illustrated to the left of figure 5 and the signal to background ratio is 1/20 (i.e. f=20). When this value is inserted in equation 2, we find that the intensity of the 3.21 MeV peak can be measured with a time resolution Δt=3.5 s at ϵ=20%.

The second emission results from the $\mathrm{t(d,\gamma)^5He}$ reaction, which is a weak branch of the main $\mathrm{t(d,n)^4He}$ fusion reaction, and is responsible for the broad structure at E_γ >10 MeV in figure 5. In $\mathrm{t(d,\gamma)^5He}$ [24], the unstable ^{5}He nucleus can be born in its ground (GS) or first excited (1L) state at 1.27 MeV. In both cases, ^{5}He has a non zero intrinsic mass width of 0.648 and 5.57 MeV, respectively. Gamma-rays at mean energies of 16.85 and 15.58 MeV are generated by the mass defect between ^{5}He and the reactants and have an intrinsic broadening determined by the non zero mass width of ^{5}He. In order to evaluate the contribution of this process to the spectrum, we have used the GENESIS code as described in [24], the $\mathrm{t(d,n)^4He}$ cross section and the branching ratio $\approx 4 \cdot 10^{-5}$ for $\mathrm{t(d,\gamma)^5He}$ measured in laser-plasma experiments by Kim et al. [25]. The uncertainty on the branching ratio is about 2 ([25, 26]) and ^{5}He has a ≈2-3 higher probability to be born in 1L with respect to GS. Of special interest for diagnostic purposes is the response of $LaBr_3$ to the high energy gamma-rays of $\mathrm{t(d,\gamma)^5He}$. According to MCNP, the interaction efficiency with the crystal is 95% and the main interaction mechanism is Compton scattering. Unlike lower energy gamma-rays, say 3-5 MeV, for which Compton scattering results in a pulse height spectrum predominantly in the region $E_\gamma < 1$ MeV, we benefit in this case from the strong forward energy peaking of the Klein-Nishina cross section that describes Compton scattering[31] and that populates the pulse height spectrum mostly in its high energy range. We find that 76% of the gamma-rays from

the t(d, γ)^{5}He reaction leave their energy in the region $E_\gamma > 10$ MeV of the pulse height spectrum, with an associated counting rate of ≈69 kHz. The independent signature of the two 16.85 and 15.58 MeV peaks in the spectrum is practically undistinguishable due to the combination of their large broadening and the Klein-Nishina cross section. As the gamma-ray background does not extend beyond E_γ >10 MeV, the time resolution at which we can measure this emission with 10% accuracy is $\Delta t \approx$ 2 - 4 ms, taking into account the uncertainty on the branching ratio of t(d, γ)^{5}He. As t(d, γ)^{5}He is the electromagnetic counterpart of t(d, n)^{4}He, this means that RGRS can also provide an independent evaluation of the neutron emission profile (albeit limited to the $r < a/3$ region) and, therefore, simultaneously study the α particle source (same as the neutron emission profile) and its slowing down.

RGRS makes use of high energy resolution spectrometers in its design, where the primary aim is to better separate the peaks of interest from the background. As demonstrated at JET [10, 12, 27], however, high energy resolution is also key to measure the peak Doppler broadening, which carries information on the α particle velocity space. To this end, the weight function formalism [28] has been recently applied to understand the velocity space sensitivity of gamma-ray emitting reactions[29, 30] by determining the probability that each region of the fast ion velocity space has to produce a gamma-ray in a specified energy bin of the pulse height spectrum. In figure 6 and 7 we show the velocity space sensitivity of the 4.44 and 3.21 MeV peaks from ^{9}Be(α, nγ)^{12}C , respectively. Results are presented for energy bins at Doppler shifts ΔE_γ =0, 15, 30 and 45 keV with respect to the nominal energies at 4439 and 3215 keV, respectively, and are obtained by multiplying the α particle slowing down distribution by the weight functions associated to each bin. The colours show the intensity of the gamma-ray emission resolved in velocity space. Low energy portions of velocity space do not emit significant intensities of gamma-rays due to the low cross sections. For the high energy portions of velocity space the weight is null because the slowing-down distribution function we have calculated does not populate the velocity-space significantly above 3.5 MeV, even though gamma-ray measurements are per se sensitive also to alphas at higher energies. For the slowing down distribution, we find for both peaks that the main gamma-ray emission occurs in rather narrow region of the velocity space, mostly at E_α=1.9 and 4 MeV for E_γ =4.44 and 3.21 MeV, respectively. These correspond to resonances of the underlying cross sections [3]. Of particular interest is the difference between weight functions corresponding to the center and tails of each peak. As already found in [29] for the 4.44 MeV emission, we here note that both peaks provide some pitch angle selectivity. In particular, channels closer to the nominal peak energy are mostly sensitive to passing ions, while the sensitivity switches mainly to trapped particles for bins in the low and high energy tails of the peak. A careful spectral measurement of the shape of both peaks therefore adds the possibility to determine the isotropy level of the α particle distribution function around the resonant energies.

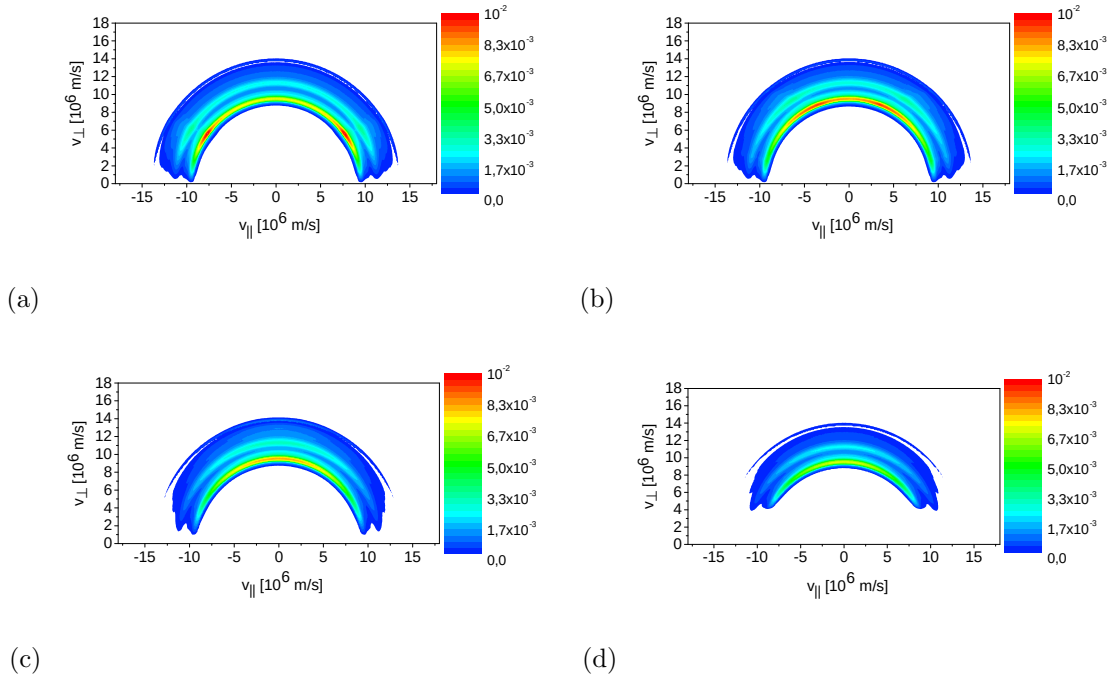

FIG. 6: Velocity space sensitivity of 4.44 MeV gamma-rays from the $^{9}\mathrm{Be}(\alpha,\mathrm{n}\gamma)^{12}\mathrm{C}$ *reaction produced at different Doppler shifts* ΔE_γ *with respect to the nominal energy* E_γ *=4439 keV. Units are* photons $\times$ s m^{-5}. ΔE_γ *= 0, 15, 30 and 45 keV, a) to d).*

5 Runaway electron studies with RGRS

5.1 Hard x-ray emission from confined runaway electrons

The second task of RGRS is to determine the energy distribution of REs at ITER through measurements of the gamma-ray spectrum in the MeV range resulting from thin target bremsstrahlung. In this section we summarise the equations that describe bremsstrahlung and that have been implemented in an extension of the GENESIS code[10, 11] to perform RGRS calculations.

The double differential cross section for the production of a gamma-ray at energy W by an electron of kinetic energy E, at an angle θ_V between the RE velocity and the emission direction and per unit solid-angle Ω can be written as [32]

$$\frac{d^2\sigma}{dW d\Omega} = \frac{d\sigma}{dW}\frac{1}{2\pi}p(Z,E,k,\cos\theta_V) \tag{6}$$

where Z is the atomic number of the target bremsstrahlung impurity and $k = W/E$. $d\sigma/dW$ indicates the energy-loss differential cross section, which is described in GENESIS based on a modified Bethe-Heitler formula (equation (49) of [33]). The main difference with respect to the pure Bethe-Heitler cross section is the inclusion of a high

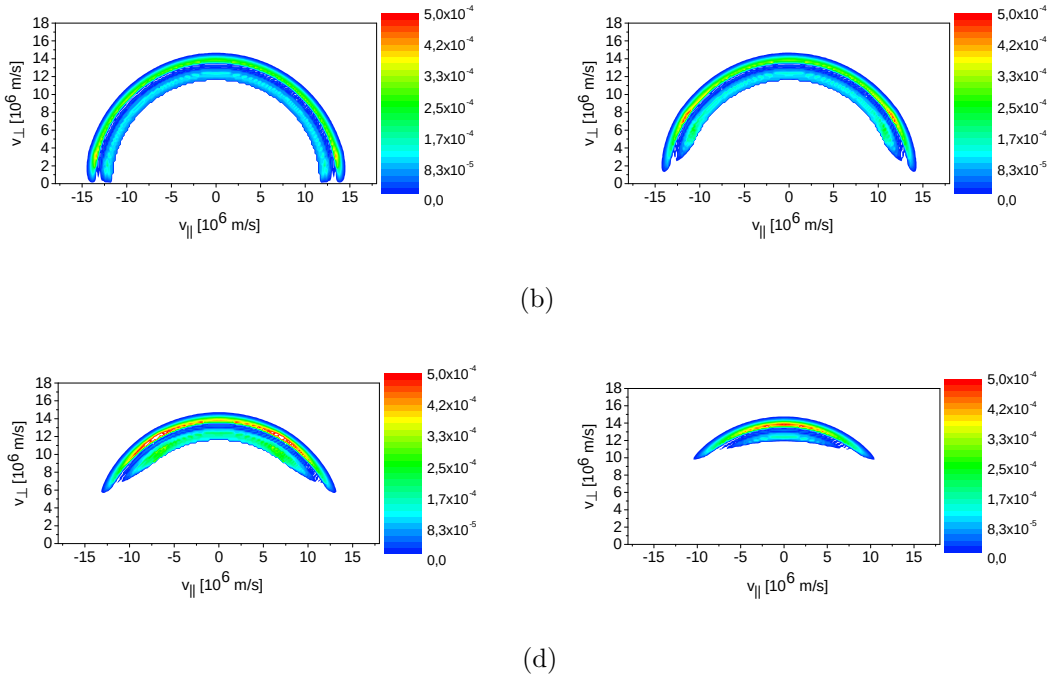

FIG. 7: Velocity space sensitivity of 3.21 MeV gamma-rays from the $^9\mathrm{Be}(\alpha,\mathrm{n}\gamma)^{12}\mathrm{C}$ *reaction produced at different Doppler shifts* ΔE_γ *with respect to the nominal energy* E_γ *=3215 keV. Units are* photons $\times$ s m^{-5}. ΔE_γ *= 0, 15, 30 and 45 keV, a) to d)*

energy Coulomb and low energy empirical corrections that have been derived in [33] based on empirical fits of the numerical results provided by Seltzer and Berger for a few elements[34, 35].

The function $p(Z, E, k, \cos\theta_V)$ is the probability distribution function of $\cos\theta_V$. When it is described by a dipole distribution in the rest frame of the runaway electron, $p(Z, E, k, \cos\theta_V)$ depends only on E and $\cos\theta_V$, i.e. $p(Z, E, k, \cos\theta_V) = p(E, \cos\theta_V)$ and

$$p(E, \cos\theta_V) = \frac{3}{16\pi}\left[1 + \left(\frac{\cos\theta_V - \beta}{1 - \beta\cos\theta_V}\right)^2\right]\frac{1}{\gamma^2(1 - \beta\cos\theta_V)^2} \tag{7}$$

Here $\beta = \sqrt{1 - 1/\gamma^2}$, where the relativistic γ is obtained from $\gamma = 1 + E/(m_e c^2)$. m_e and c indicate the electron mass and speed of light, respectively.

Figure 8 shows an example of $d\sigma/dW$ and $p(E, \cos\theta)$ for E =1 and 10 MeV REs. Here we note that, as expected, the bremsstrahlung cross section is larger by $10^4 - 10^5$ times at $k << 1$ with respect to $k \approx 1$. The emission is mostly along the direction of the RE velocity and decreases by 4-5 orders of magnitude for $\cos\theta_V \approx 0$, which is the emission angle of relevance for RGRS when bremsstrahlung radiation is produced by the strongly passing REs.

Equations 6, 7 and (29) of [33] provide a relatively simple analytical representation

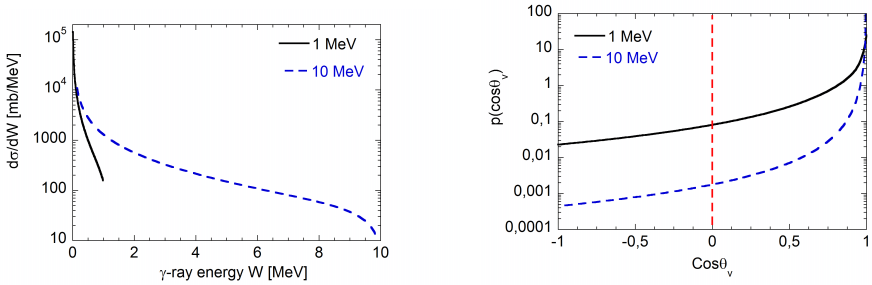

FIG. 8: (left) Differential cross section for the production of gamma-rays as a function of the gamma-ray energy (right) Angular probability of gamma-ray emission as a function of the cosine of the angle between the line of observation and the runaway electron velocity. Results are shown for 1 and 10 MeV runaway electrons. The red dashed line indicates the angle of observation of the RGRS system.

of the double differential cross section for bremsstrahlung emission and are particularly suitable for Monte Carlo sampling such as needed in GENESIS. In order to understand the accuracy of these approximations we have compared the calculations of GENESIS with those of MCNP, which implements instead the most accurate numerical tables of Seltzer and Berger [34, 35], including a correction to the dipole distribution at low electron energies (<500 keV). Figure 9 shows the bremsstrahlung emission spectrum generated by mono energetic electrons at 5 and 10 MeV that collide with bulk ^{20}Ne at a unit density of 1 m^{-3}. Gamma-rays are emitted at 90° with respect to the electron velocity and in a solid angle $\Delta\Omega = 2\pi\Delta\theta_V$ with $\Delta\theta_V$=2° . The agreement between the two calculations is very good, especially in the region E_γ >1 MeV, and GENESIS results have a significantly lower fluctuation level with respect to MCNP when the same number of samples is used, thanks to the simplicity of the analytical formulas of [33]. Concerning the intensity of the emission, there is only a slight mismatch up to about 30% between MCNP and GENESIS for E_γ <500 keV. This is however of no concern as gamma-ray measurements in a tokamak are typically performed with a low energy threshold of about 500 keV in order to avoid low voltage noise pick up on the cables as well as to cut the intense background emission at 511 keV from the spectrum. The latter arises from the annihilation of positrons produced by the interaction of gamma-rays with the shielding materials surrounding the detector and is undesired in the spectrum.

5.2 Physics studies

Information on the energy distribution of RE electrons resides in the shape of the HXR spectrum from bremsstrahlung emission. Unlike the ^{9}Be$(\alpha, \mathrm{n}\gamma)^{12}$C reaction, which emits in a narrow energy interval of ≈ 100 keV around the two nominal energies 3.21 and 4.44 MeV, the HXR spectrum is extended over a rather large energy range, say some tens of MeV, and is generated on the typical time scale of a disruption, say $\tau_d \approx 100$ ms. The aim of RGRS is therefore to measure the shape of the HXR spectrum with a time resolution $\Delta t \approx \tau_d/10$. In order to evaluate the performance of RGRS against RE measurements,

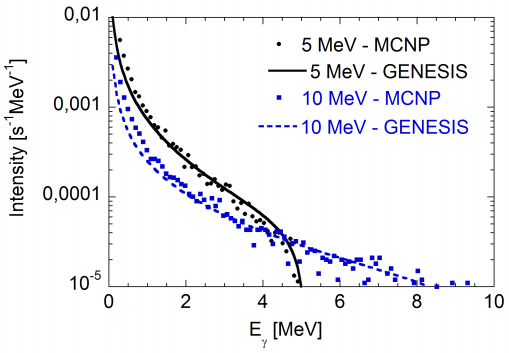

FIG. 9: Comparison of the bremsstrahlung emission spectrum generated by mono energetic electrons at energies of 5 and 10 MeV as calculated by the MCNP and GENESIS codes. Gamma-rays are emitted at 90° with respect to the electron velocity and in a solid angle $\Delta\Omega = 2\pi\Delta\theta_V$ *with* $\Delta\theta_V$=2° *. The emission arises from collisions with* ^{20}Ne *with unit density (*1 m^{-3}*).*

we have used GENESIS to calculate the HXR spectrum expected in a disruption scenario at different levels of the RE current I_{RE}. In all cases, we have assumed an exponential runaway electron distribution of strongly passing (pitch=1) REs with mean energy 12.5 MeV and minor radius of 1 m for the RE beam [36]. Under these conditions, the average RE velocity is $v_{RE} \approx 0.98 \cdot c$ and the runaway electron density n_{RE} is proportional to the current I_{RE} through

$$n_{RE} = \frac{I_{RE}}{q v_{RE} \pi a^2} \tag{8}$$

where a =1 m is the RE beam radius. As the HXR emission is also proportional to n_{RE}, the signal from REs scales linearly with I_{RE}.

Calculations have been performed for scenarios with and without the injection of external impurities to mitigate the RE beam [37] with details given in Table II. Figure 10 shows an example of the bremsstrahlung spectrum produced by a point at the centre of the RE beam and when the radiation is emitted at 90° towards the RGRS detectors. The calculation refers to the case of an extreme runaway current I_{RE}=10 MA (and that can be compared with a plasma current of 15 MA expected in steady state scenarios at ITER) and for the unmitigated scenario of Table II. In all of the other scenarios, the shape of the spectrum is very similar and it is mostly the intensity that is different, especially when large amounts of ^{20}Ne are used. The mean spectral energy $< E_\gamma >$ is about 100 keV, showing that most of the emission involves gamma-rays at energies significantly lower than those of the REs, in agreement with the cross sections of figure 8. The counting rates measured by the central channel of the RGRS detectors when I_{RE}=10 MA are reported in Table II.

The RE distribution function, as well as its current, can be obtained from the measured spectrum by a deconvolution method that takes into account both the HXR emission process and the response function of the detector. The method is extensively described in [5]. A study on the possible systematic errors that can affect the reconstruction of the

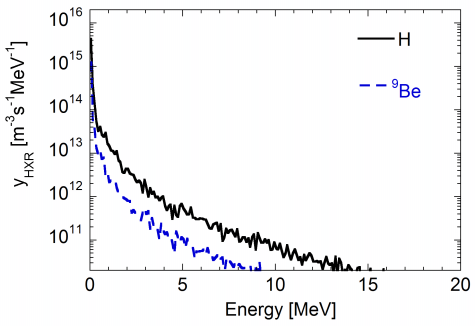

FIG. 10: Simulated gamma-ray emission spectrum impinging on the RGRS system at ITER from runaway electrons in a non mitigated disruption when the runaway current is 10 MA. The y axis indicates the emissivity in the plasma center for gamma-rays emitted towards the RGRS detectors. The bremsstrahlung emission spectrum from collisions with hydrogen and ^{9}Be is separately shown.

TABLE II: Disruption scenarios and results on the counting rate expected at the RGRS detectors as simulated with the GENESIS code. Small and large injection refer to a disruption scenario that is mitigated by the introduction of impurities in the plasma. I_{RE}=10 MA is assumed in all cases.

Scenario	Impurity species	Impurity density (10^{20} m^{-3})	Hydrogen density (10^{20} m^{-3})	Counting rate [Hz] ($E_\gamma > 500$ keV)
Unmitigated	Beryllium	0.01	0.5	$1.0 \cdot 10^6$
Small injection	Neon	0.05	1.0	$6.4 \cdot 10^6$
Large injection	Neon	25.0	0.5	$2.4 \cdot 10^8$

RE distribution has been carried out in [6] and, in particular, it is estimated that the spectrum should be made by at least $N_C = 10^4$ counts to avoid artefacts in the reconstructed RE distribution. By considering this constraint, we find that RGRS can provide time resolved measurements of the RE distribution with Δt=10 ms at I_{RE}= 10 MA in the unmitigated scenario or, alternatively, a time integrated spectrum (Δt=100 ms) down to I_{RE} =1 MA. Some impurity injection is required to cover the lowest I_{RE} scenarios or to obtain time resolved measurements at I_{RE} <1 MA. In the large injection scenario, I_{RE} as low as 40 kA provides a HXR spectrum with $N_C = 10^4$ every Δt=10 ms, but the counting rate becomes unacceptably high to operate the detectors when $I_{RE} > 400$ kA. In summary, depending on the level of the injected impurity that is used, measurements of the HXR spectrum by RGRS in a large I_{RE} range between 40 kA and 10 MA are possible with a time resolution Δt=10 ms. In all of our evaluations we have not considered the neutron background arising from photo-dissociation. This is, however, at a typical level of 10-20%, i.e. negligible within the accuracy of our calculations.
As for the ^{9}Be$(\alpha, n\gamma)^{12}$C reaction, we could use weight functions to understand the veloc-

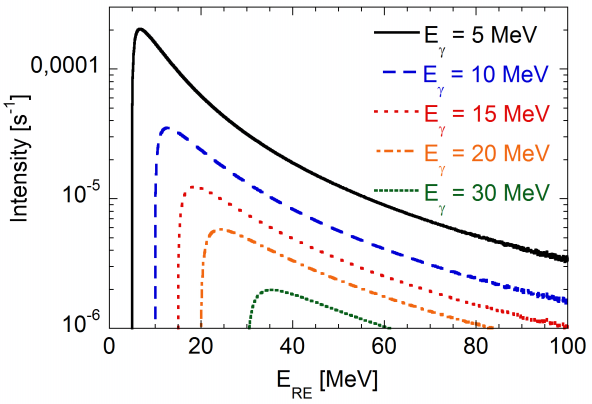

FIG. 11: Probability that a gamma-ray at energy W is generated by a strongly passing (pitch = 1) RE with energy E_{RE}. The bulk plasma has density $n_e = 10^{20}$ m^{-3} and no impurity injection is assumed. Gamma-rays are emitted at 90° with respect to the magnetic field.

ity space sensitivity of HXR measurements. For bremsstrahlung emission, however, full weight functions have not yet been derived and are outside the scope of this paper. Here we limit ourselves to apply the numerical method described in [29] to strongly passing (pitch=1) REs and when photons are emitted at 90° with respect to the electron (or, equivalently, to the magnetic field). The result is a slice of the full weight function on the $v_\perp = 0$ axis (or on the pitch=1 axis) and gives the intensities that REs at various energies E_{RE} generate at particular gamma-ray energies of the measured spectrum. Figure 11 shows the outcome for E_γ=5, 10, 15, 20 and 30 MeV. Since energy has to be conserved, gamma-rays at E_γ cannot be born from REs with $E_{RE} < E_\gamma$, which explains the sharp drop that each curve has when $E_{RE} = E_\gamma$. The shape of the probability curve resembles that of an electronic pulse, with a peak in close vicinity of $E_{RE} = E_\gamma$ and a long tail that extends to higher E_{RE}. In other words, photons at E_γ are mainly sensitive to runaways at energies $E_{RE} \approx E_\gamma$, but can also carry some information on higher energy electrons. Of particular interest is the magnitude of the maximum of each probability curve as a function of E_γ. By comparing, for instance, the results for E_γ =5 and 30 MeV, we find that the intensity of the maximum decreases by a factor ≈ 100, while the detection efficiency of E_γ =5 and 30 MeV by $LaBr_3$ is practically the same. The reason is the progressively higher forward peaking of bremsstrahlung emission as the electron energy is increased, as shown by the dipole distributions of figure 8, at the expense of the emission at 90°. For practical applications, it is this forward peaking of the bremsstrahlung emission that sets an upper limit to the RE energy at which RGRS can be sensitive and that we identify to be E_{RE} ≈30-40 MeV, based on the intensity of the peak in figure 11 and considering that a dynamic range of 2-3 orders of magnitudes at most is experimentally viable with $LaBr_3$.

In principle, the sensitivity to higher energy REs could be recovered by performing measurements along a line of sight in the direction of the runaway electron beam. Figure 12

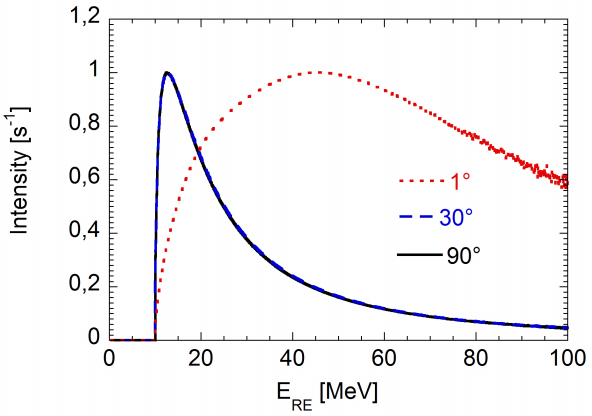

FIG. 12: Probability that a gamma-ray at energy 10 MeV is generated by a strongly passing (pitch = 1) RE with energy E_{RE} as a function of the observation angle between the magnetic field and the detector. The bulk plasma has density $n_e = 10^{20}$ m^{-3} and no impurity injection is assumed. The maximum of each curve is normalised to 1.

shows the probability that 10 MeV gamma-rays are generated by strongly passing (pitch = 1) RE with energy E_{RE} and at a different observation angles ϕ between the magnetic field and the detector. The maximum of each curve is normalised to 1. We find that, when the observation angle is 1° , the sensitivity peaks at $E_{RE} \approx 50$ MeV and the maximum is very broad. On the other hand, there is no difference between the two curves when ϕ =30° or 90°. Therefore, it is only by observing the beam at very grazing angles that the runaway electron sensitivity can be extended beyond E_{RE} ≈30-40 MeV. However, due to the cross sections of figure 8, we also find that the intensity of the emission for ϕ=1° is about 10^6 times higher than that at ϕ=90° , which suggests that HXR measurements along lines of sight at very grazing angles are very difficult to exploit without saturating the detector already at $I_{RE} < 1$ kA.

6 Discussion

Besides RGRS, the present set of diagnostics for the energy distribution of confined fast ions at ITER includes Collective Thomson Scattering (CTS) [38], Neutral Particle Analyzer (NPA) [39] and a High Resolution Neutron Spectrometer (HRNS) [40]. Of these 3 systems, only CTS and NPA have been developed to measure alpha particles. The CTS diagnostics is active and relies on the injection of microwaves in the plasma and their collective scattering by a selected observation volume in the plasma. CTS measurements of fast ions born from beam or radio-frequency heating have been demonstrated in deuterium plasmas at JET[41], TEXTOR [42], ASDEX-Upgrade [43, 44] and LHD[45], but no measurement in deuterium-tritium plasmas is available to date and will be accomplished for the first time at ITER.
NPA is based on the charge exchange between deuterons from neutral beam injection and the bulk plasma. Measurements of alpha particles are indirect and are made possible by

the detection of deuterium neutrals with energies above that of the beam and which are born from the nuclear elastic scattering collisions between α particles and bulk deuterium [46]. The possibility to disentangle the α particle energy distribution from the measured knock on deuterons relies on modelling of nuclear elastic scattering and transport of neutrals from the plasma core to the detector. Presently, the NPA diagnostic is planned on a single line of sight and no profile information can be provided with this system.
In this context, RGRS is based on gamma-ray spectroscopy, which has been already demonstrated in JET deuterium plasmas with and without tritium [2, 4], and can complement CTS measurements of the slowing down α particle profile. In terms of studies of the α particle energy distribution, RGRS provides information on α particles in narrow energy windows around the resonances of the underlying cross sections, i.e. mostly 1.9 and 4 MeV. The very different shapes of the CTS and GRS weight functions suggests that the measurements will complement each other very well [47]. Careful analysis of the Doppler broadened peak shape of the gamma-ray emissions can give some insight on the isotropy of the distribution function. A unique feature of RGRS, which is not shared by CTS and NPA, is its capability to simultaneously observe the α particle source and its slowing down.
Concerning runaway electron measurements, the present set of diagnostics at ITER consists mainly on wide angle infra-red cameras, which are developed for machine protection by the detection of hot spots associated to particle losses to the first wall. The development of a synchrotron radiation diagnostic [48] based on infra-red emission and that can add some information on the runaway electron energy distribution has been proposed but is currently not under development. In this context, RGRS has an even more important role at ITER as, together with the gamma-ray diagnostic system behind the NPA [49], will be the only system that can measure the runaway electron energy distribution on a time scale of 10 ms and their spatial profile in the $r < a/3$ region.
In terms of meeting the primary requirements of gamma-ray spectrometry in table I, we find that RGRS as designed fully satisfies the needs for runaway electron measurements, albeit with a sensitivity to the runaway electron distribution up to $\mathrm{E_{RE}} = 30 - 40$ MeV. In terms of α particle measurements, time resolution and accuracy requirements are met when the core α particle density is $\geq 10^{18}$ m^{-3} as for the parameters specified in [18] and used in this study. Lower α particle densities may also be accessible without degrading the time resolution of the measurements, depending on the ^{9}Be concentration available in the machine. The spatial coverage of the measurements is instead limited to the core $r < a/3$ region in the present design, as no gamma-ray detectors are envisaged for installation in the in-port region.

7 Conclusions

In this paper the principles behind the design of the Radial Gamma Ray Spectrometers (RGRS) system for alpha particle and runaway electron (RE) measurements at ITER have been presented, together with an assessment of the system at a conceptual level. By combining the most advanced detector solutions available for tokamak plasmas, RGRS can

combine space and energy distribution measurements of α particles and REs in a single diagnostic. With our design choices, we are capable to provide α particle measurements by detection of the associated 4.44 MeV gamma-ray emission on a time scale of the order of 1/10 of the α particle slowing down time for the 500 MW full power DT phase of ITER. The E_γ >10 MeV emission from the $\mathrm{t(d,\gamma)^5He}$ reaction is measured with 2-4 ms time resolution and provides an independent determination of the neutron profile, which coincides with the α particle source. RGRS can therefore study simultaneously the birth and slowing down of the α particles. Spectroscopy measurements of the 3.21 and 4.44 MeV peaks on a second time scale make gamma-ray emission sensitive to possible anisotropies of the α particle distribution and are representative of alphas around the resonant energies of the underlying $^9\mathrm{Be}(\alpha,\mathrm{n}\gamma)^{12}\mathrm{C}$ cross sections, i.e. mostly 1.9 MeV and 4 MeV for the two peaks, respectively.
The detection of bremsstrahlung emission in the MeV energy range makes RGRS capable to determine the energy distribution of runaway electrons for I_{RE} between 40 kA and 10 MA, where the range I_{RE} <400 kA is accessed by means of gas injection, for example ^{20}Ne , and with a time resolution of 10 ms. The sensitivity of HXR measurements to the runaway electron energy distribution is up to E_{RE} ≈30-40 MeV, where the upper limit is determined by the increasing forward peaking of the dipole distribution that describes bremsstrahlung. This compares to an expected duration of the disruption of 100 ms.
Compared to other diagnostics currently planned for confined α particle measurements at ITER, the role of RGRS is to complement and independently benchmark the results of the NPA and CTS. A more unique role can be identified as far as HXR measurements are concerned, as spectral studies of bremsstrahlung emission are the only way presently envisaged to determine the energy distribution of runaway electrons at ITER.

8 Acknowledgments

The work leading to this publication was funded partially by Fusion for Energy under the Specific Grant Agreement F4E-FPA327-SG04. This publication reflects the views only of the authors, and Fusion for Energy cannot be held responsible for any use which may be made of the information contained therein. The views and opinions expressed herein do not also necessarily reflect those of the ITER Organization.

References

[1] KIPTILY V.G. et al. Nucl. Fusion 42 (2002) 999

[2] KIPTILY, V.G. et al. Plasma Phys. Control. Fusion 48 (2006) R59-R82

[3] KIPTILY, V.G. et al. Rev. Sci. Instrum. 74 (2003) 1753

[4] TARDOCCHI M. et al. Plasma Phys. Control. Fusion 55 (2013) 074014

[5] SHEVELEV A.E. et al. Nucl. Fusion 53 (2013) 123004

[6] SHEVELEV A.E. et al. Nucl. Instrum. Meth. A 830 (2016) 102

[7] A.J.H DONNE' et al. Nucl. Fusion 47 (2007) S337–S384

[8] G. VAYAKIS et al. "Evolution of the ITER Diagnostic Set Specifications", 24th IAEA Fusion Energy Conference Contribution (IAEA-CN–197), San Diego, USA, October 8–13, 2012, ITR/P5-37

[9] MAROCCO D. et al. "System Level Design and Performances of the ITER Radial Neutron Camera", These Proceedings

[10] TARDOCCHI M. et al. Phys. Rev. Letters 107 (2011) 205002

[11] NOCENTE M. et al. "Neutron and gamma-ray emission spectroscopy as fast ion diagnostics in fusion plasmas", PhD Thesis, 2012, available online at https://boa.unimib.it/handle/10281/28397

[12] NOCENTE M. et al. Nucl. Fusion 52 (2012) 063009

[13] NOCENTE M. et al. Rev. Sci. Instrum. 81 (2010) 10D321

[14] NOCENTE M. et al. IEEE Trans. Nucl. Sci. 60 (2013) 1408

[15] NOCENTE M. et al. Rev. Sci. Instrum. 87 (2016) 11E714

[16] RIGAMONTI D. et al. Rev. Sci. Instrum. 87 (2016) 11E717

[17] ZYCHOR I. et al. Phys. Scr. 91 (2016) 064003

[18] POLEVOI A., "Assessment of Neutron Emission from DD to DT operation of ITER", IDM UID Q43JH7

[19] NOCENTE M. et al. Nucl. Fusion 51 (2011) 063011

[20] BATISTONI P. et al. Rev. Sci. Instrum. 66 (1995) 4949

[21] CAZZANIGA C. et al. Nucl. Instrum. Meth. A 778 (2015) 20

[22] CHUGUNOV I. et al. Instruments and Experimental Techniques 51 (2008) 166

[23] VANDEVENDER B.A. et al. IEEE Trans. Nucl. Sci. 61 (2014) 2619

[24] NOCENTE M. et al. Nucl. Fusion 55 (2015) 123009

[25] KIM Y. et al. Phys. Rev. C 85 (2012) 061601

[26] CECIL F.E. et al. Phys. Rev. C 32 (1985) 690

[27] ERIKSSON J., NOCENTE M. et al. Nucl. Fusion 55 (2015) 123026

[28] M. SALEWSKI et al. Nucl. Fusion 52 (2012) 103008

[29] M. SALEWSKI et al. Nucl. Fusion 55 (2015) 093029

[30] M. SALEWSKI et al. Nucl. Fusion 56 (2016) 046009

[31] KNOLL G. F. "Radiation detection and Measurements", 4th Edition, ed. Wiley, 2010, chapter 10

[32] SALVAT F. and FERNANDEZ-VAREA J.M. Nucl. Instrum. Meth. B 63 (1992) 255

[33] SALVAT F et al. Radiation Physics and Chemistry 75 (2006) 1201

[34] SELTZER S.M. and BERGER M.J. Nucl. Instrum. Meth. B 12 (1985) 95

[35] SELTZER S.M. and BERGER M.J. Data Nucl. Data Tables 35 (1986) 345

[36] LEHNEN M. Private Communication

[37] PAUTASSO G. et al. Nucl. Fusion 55 (2015) 033015

[38] SALEWSKI M. et al. Nucl. Fusion 49 (2009) 025006

[39] AFANASYEV V.I. et al. Nucl. Instrum. Meth. A (2010) 456

[40] HELLESEN C. et al. "Conceptual Design of the Best TOF Neutron Spectrometer for Fuel-Ion Ratio Measurements at ITER", These Proceedings

[41] BINDSLEV H. et al. Phys. Rev. Lett. 83 (1999) 3206

[42] MOSEEV D. et al. Plasma Phys. Control. Fusion 53 (2011) 105004

[43] SALEWSKI M. et al. Nucl. Fusion 50 (2010) 035012

[44] JACOBSEN A. et al. Plasma Phys. Control. Fusion 58 (2016) 042002

[45] NISHIURA M. et al. Nucl. Fusion 54 (2014) 023006

[46] KOROTKOV A.A. et al. Physics of Plasmas 7 (2000) 957

[47] SALEWSKI M. et al. Nucl. Fusion 51 (2011) 083014

[48] JASPERS R. et al. Rev. Sci. Instrum. 72 (2001) 466

[49] GIN D. et al. "Gamma Ray Spectrometer for ITER", AIP Conference Proceedings 1612 (2015) 149